Conductivity and structural properties of fast Ag-ion-conducting GaGeSbS–AgI glassy electrolytes

Bitner M.A., Qing Jiao, Y. Zhang, C H. Lin, Xianghua Zhang, H. Ma, T S. Dai, G. B. Jia

Conductivity and Structural Properties of Fast Ag-Ion-Conducting GaGeSbS−AgI glassy Electrolytes

Baochen Ma[1], Qing Jiao[1*], Yeting Zhang[1], Changgui Lin[1], Xianghua Zhang[2], Hongli Ma[2], Shixun Dai[1]

[1] Laboratory of Infrared Material and Devices, Advanced Technology Research Institute, Ningbo University, Ningbo, Zhejiang, 315211, China

[2] Laboratory of Glasses and Ceramics, Institute of Chemical Science, UMR CNRS 6226, University of Rennes 1, Rennes, France

Keywords: Sulfide solid electrolyte, Superionic conductor, Electrochemical behavior, AC impedances spectroscopy

Abstract

The use of ion-conducting chalcogenide glass, a promising solid electrolyte, is encouraged at higher conductivity for all-solid-state rechargeable battery. Herein, a new quaternary glass of GaGeSbS–AgI system was successfully prepared, and its structural and electrochemical properties were investigated by XRD, Raman, and AC impendence measurement. The relatively high conductivity of 2.955×10^{-3} S/cm and low activation energy of 0.07 eV were obtained after optimized structure regulation. The short-range schematic of the glass structure was explored to determine the fast-migrating mechanism involved in conducting Ag^+ ions. By controlling the proper ratio of Ga(Ge) and Sb cations, the loose and porous layer structure of $[SbS_xI_{3-x}]$ linking by the $[Ga(Ge)S_4]$ tetrahedron was formed, resulting in the rapid transport of Ag^+ ions with a reduced migration energy barrier. The current work is the first time that a sulfide solid electrolyte in quaternary glass system with desirable electrochemical characteristics was used to address energy and safety issues.

1. Introduction

The improvement of global human living standards has led to a huge demand for energy consumption, especially for hybrid electric vehicles and portable energy storage devices[1-4]. Traditional lithium-ion liquid batteries have been widely used in the commercial market due to their qualified energy density (≈ 250 Wh/kg)[5-7]. Nevertheless, owing to the frequent reports of liquid electrolyte leakage and thermal instability, the simultaneous achievement of high power and safety in current electrochemical devices seemed impossible[8, 9]. Therefore,

all-solid-state batteries with inorganic electrolytes have the potential to solve the problems related to safety and high energy density[10]. Sulfide solid glass electrolytes have become the focus of research because of their superior properties, such as high polarization and large ionic radius of S^{2-}, which effectively improve ionic diffusion and room temperature conductivity. Meanwhile, the conduction pathways are isotropic and flexible due to the absence of crystalline passageways in the network. Ionic transport is accelerated by the amorphous network without grain boundary, contributing to the increase in ionic conductivity by several orders of magnitude compared with crystallines[11]. Moreover, sulfide glass with loosened transport channels and low binding energy is considered a candidate ionic conductor in producing efficient solid electrolytes[12].

However, the low ionic conductivity of solid electrolytes hinders the performance of solid-state batteries. Hence, the exploration of sulfide electrolytes with excellent room-temperature ionic conductivity has become a significant challenge in terms of system design and structural optimization in recent years. The glass former (GeS_2, As_2S_3, Sb_2S_3) doped with metal compounds, including alkali-metal ions Li^+, Na^+, and K^+ and transition-metal ions Ag^+ and Cu^+, was chosen for the solid electrolyte because of its good glass-forming ability and electrochemical properties[13-15]. The ternary glass system formed by aliovalent cations doping, such as GeGaS and GeSbS, is widely studied. In 2008, the conductivity of $(100-2x)GeS_2–xGa_2S_3–xAgI$ (1.2×10^{-6} S/cm) was reported by Stehilk et al.[16]. Then, the conductivity of AgI-doped GeSbS ternary glass system was raised to the commercially available magnitude of 10^{-3} S/cm through the regulation of the Ge/Sb ratios in the glass matrix[12]. One of the effective ways to improve ionic conductivity is aliovalent ion substitution. The charge-compensating induction vacancies or interstitials increased the degree of disorder in the matrix, which benefits the carrier's long-range diffusion through the glass network. The control preparation of the sulfide glass materials and the design of the ions' migration pathways are promising measures that can be used to achieve higher ion conductivity for secondary batteries.

In this work, two series of glass samples $60[x(Ga_2S_3–3GeS_2)–(1-4x)Sb_2S_3]–40AgI$ and $(100-y)(0.1Ga_2S_3–0.3GeS_2–0.6Sb_2S_3)–yAgI$ were prepared by melt quenching method. The optimized ionic channel was expected to obtain from the composition design aiming to achieve the high ionic conductivity with increasing silver dopant concentration. Germanium sulfide is used as a virtuous network former to easily form glasses with or without other alloy compounds. The mixed-cation effect, such as that in Sb_2S_3 and Ga_2S_3 sulfides, further enhances conductivity and stability with controlled coordination polyhedrons in the Ag ion conductive glass. The GaGeSbS–AgI glass system in the current work has a wide glass-forming region and favorable ionic conductivity of 2.95×10^{-3} S/cm, which is higher than those of most sulfide electrolytes doped with halide salt. This work is our first attempt to synthesize a sulfide solid electrolyte in a quaternary glass system with desirable electrochemical characteristics.

2. Experimental

The samples of the system $60[x(Ga_2S_3–3GeS_2)–(1-4x)Sb_2S_3]–40AgI$ (A-series, x = 0.1, 0.15, 0.2 mol%) and $(100-y)(0.1Ga_2S_3–0.3GeS_2–0.6Sb_2S_3)–yAgI$ (B-series, y = 50, 55, 60 mol%) were prepared by conventional melt quenching technique in sealed silica ampules ($\sim 10^{-3}$ Pa) with high-purity materials including Ga, Ge, Sb, S, and AgI compounds[17]. The batches of about 15 g were heated to 950 °C for 12 h, quenched and then annealed. The obtained rod-like glass was processed into 10- and 2 mm- thick discs. The samples of A-series were abbreviated as $(GG)Sb_z$ (z = 0.2, 0.4, 0.6).

Confirmation of crystallographic and amorphous state of the prepared sample was performed by XRD measurement (Bruker D2 Phaser; Cu Kα; 10 mA, 30 kV). The calorimetric measurement was performed using DSC (TA Q2000 Thermal Analysis) with a scan rate of 10 °C/min. The prepared disc was polished optically and then sputtered with Au for electrochemical tests. The as-prepared samples were evaluated using AC impedance method for ionic conductivity at 30 °C–100 °C and 1 Hz–1 MHz. Structure detection was conducted at room temperature using a Raman spectrometer with a 785 nm LD laser (Renishaw inVia,

Gloucestershine, UK).

3. Results and Discussion

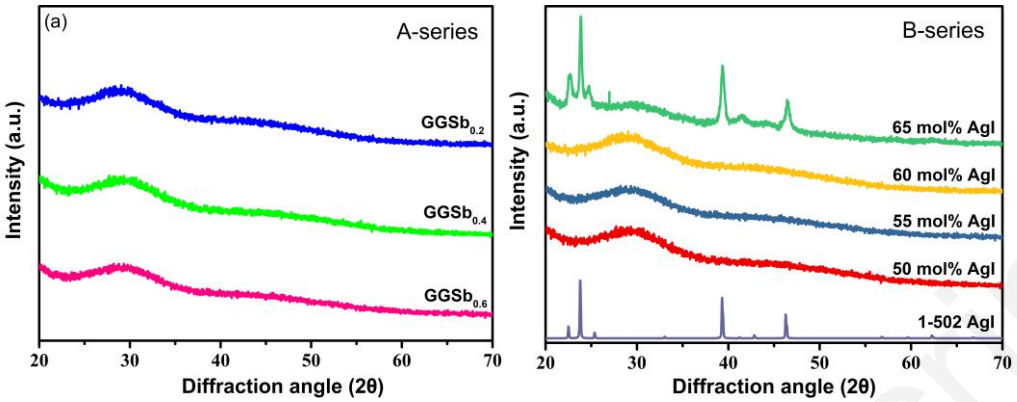

Fig.1. XRD patterns of the as-prepared 60[x(Ga_2S_3–3GeS_2)–(1-4x)Sb_2S_3]–40AgI samples in the A-series (a), and (100-y)(0.1Ga_2S_3–0.3GeS_2–0.6Sb_2S_3)–yAgI samples in the B-series (b).

Fig. 1 shows the XRD patterns of all the samples. Three diffraction spectral lines with typical halo pattern are shown in Fig. 1 (a), thereby confirming the amorphous state of the A-series samples. In the Fig. 1 (b), an extensive crystalline peak occurred in the B-series when 65 mol% AgI was added into the matrix. Several peaks appeared at the diffraction locations following 22.5°, 23.7°, 25.2°, 39.3°, and 46.3°, which can be ascribed to the standard β/γ-AgI crystals (JCPDF card of no.1-502).

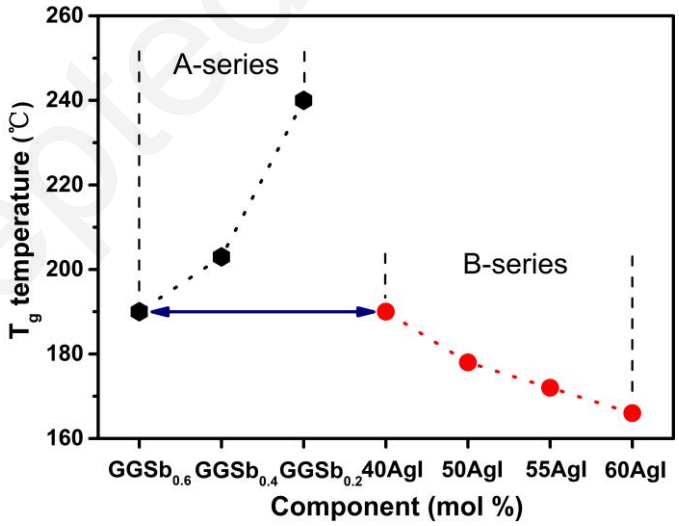

Fig. 2. The variation tendency of T_g obtained from the DSC measurement.

Thermodynamic properties of as-prepared samples were investigated by DSC detection in Fig. 2. In the case of A-series, the values of T_g presented a rising trend with increasing addition of Sb_2S_3 component, and this trend was related to the intensified degree of cross-linking network.

The tetra-coordinated [Ga(Ge)S_4] units in the matrix provided more covalent bonding connections than tri-coordinated [SbS_3] units, resulting in a higher degree of network linkages. Meanwhile, the elimination of non-bridging sulfurs (NBS) in the network enhanced the interconnections between the structural units. However, in the case of the B-series, I^- ions were introduced into the matrix to serve as network terminator, which reduced the compactness of the glass network[18]. Eventually, the T_g of the 60 mol%-doped AgI sample became well maintained at 166 °C, indicating that a high operating temperature can be realized in this glass electrolyte.

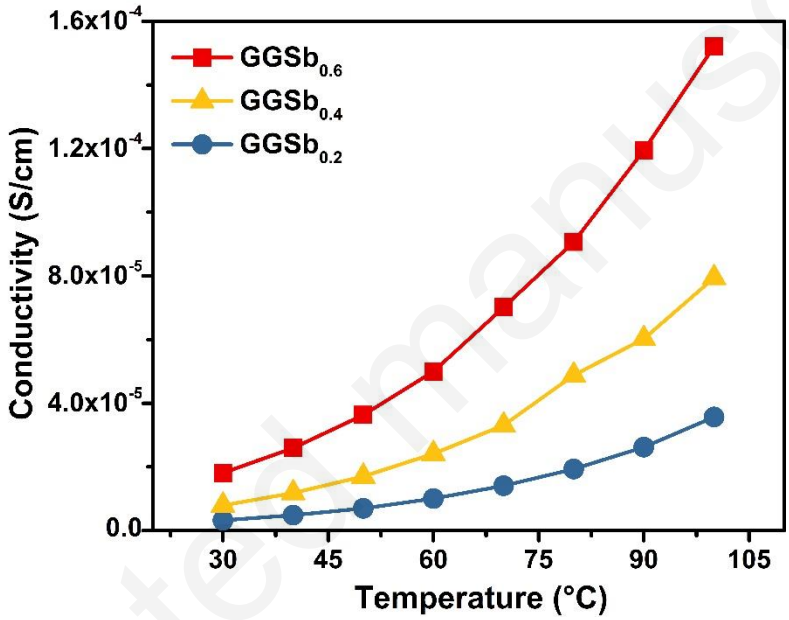

Fig. 3. The conductivity of A-series sample with different temperatures from 30 °C to 100 °C.

Fig. 3 presented the ionic conductivity of A-series samples as a function of temperature. The calculated conductivity of each sample was obtained from the relationship of $\sigma=R^{-1}D/S$, where D is the sample thickness, and S represents the gold-coated area of the electrodes. High room temperature conductivity (2×10^{-5} S/cm) was obtained in (GG)$Sb_{0.6}$ sample of A-series, which reveals the optimized component for the improvement of ionic conductivity. With increasing temperature, the conductivity of all the A-series samples showed a significant enhancement. However, the differences in the increase in amplitude indicated the intrinsic differences of the ionic channels for the designed samples.

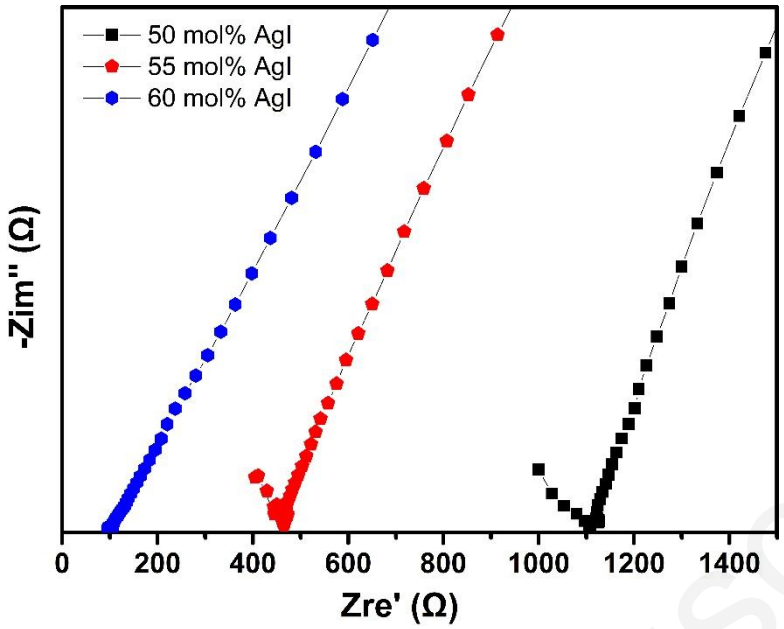

Fig. 4. Typical Nyquist diagram of the (100-*y*)(0.1Ga_2S_3–0.3GeS_2–0.6Sb_2S_3)–*y*AgI samples in the B-series (*y* = 50, 55, 60 mol %).

The representative Nyquist plot of B-series samples with different concentrations of AgI is given in Fig. 4, where *Zre′* and *-Zim″* represent the resistance and reactance of bulk-samples, respectively. The presence of a semicircle (or half) and a spike, which indicated the typical behavior of an ionic conductor, was observed in the high- and low-frequency regions of the current. Lower resistance was realized with increasing ionic Ag^+ content, leading to an excellent room temperature conductivity of 2.955×10^{-3} S/cm in the 60 mol% AgI sample. In general, the samples showed good fitting according to the Arrhenius Law, which was expressed as follows:

$$\sigma = Aexp(-\frac{E_a}{RT})$$

where A is the pre-exponential factor, R is the Boltzmann constant, T is the absolute temperature, and E_a is the activation energy. In theory, the barrier energy associated with optimized migration path was characterized by the magnitude of the E_a. The E_a values of samples doped with 50, 55, and 60 mol% AgI were calculated to be 0.1, 0.08, and 0.07 eV, respectively, which were relatively lower value compared with those of other sulfide solid electrolytes, such as GeSbSe–Ag (0.32 eV) and GeGaSe–AgI (0.28 eV) glass systems[15, 19].

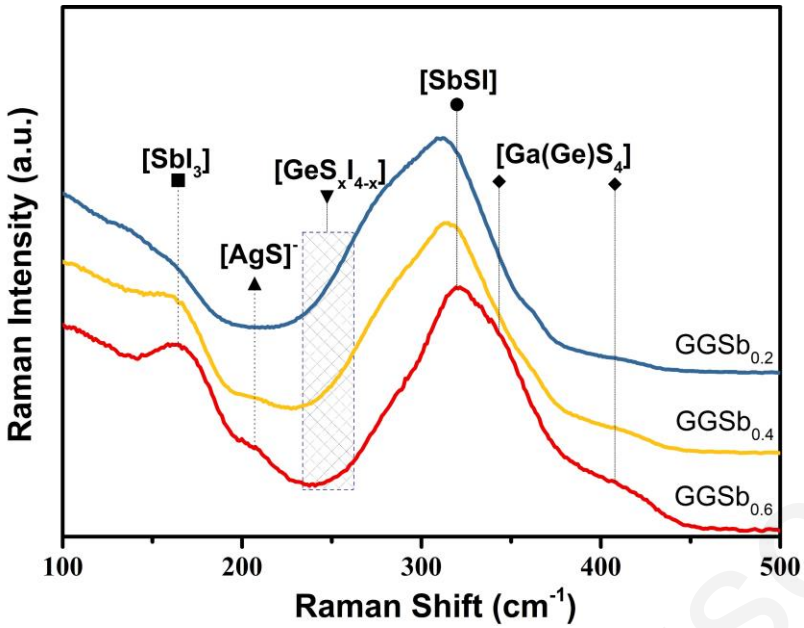

Fig. 5. Raman spectra of $60[x(Ga_2S_3–3GeS_2)–(1-4x)Sb_2S_3]–40AgI$ (A-series, x = 0.1, 0.15, 0.2 mol) samples.

To explore the effect of the structure nature of the sample on the conductivity characteristic, the samples were subjected to the Raman test. The obtained Raman spectrum of A-series samples is shown in Fig. 5; it consists of a broad band between 100 and 500 cm^{-1}. Considering the significant changes of the ionic channels, the detailed analysis of the spectra was divided into Sb-related and Ga(Ge)-related vibrations. For $(GG)Sb_{0.2}$ sample, the primary peak near 308 cm^{-1} was attributed to the vibrations of [SbSI] units. However, the peak position shifted to a higher wavenumber at 318 cm^{-1} with increasing Sb_2S_3 in the network. Moreover, the band near 162 cm^{-1}, which belongs to $[SbI_3]$ units, appeared with the increased substitution of the Sb_2S_3 component. On the contrary, the peak shoulder from 230 cm^{-1} to 260 cm^{-1} represented the structural units of $[GeS_xI_{4-x}]$, thereby increasing the vibration dependence of the Ge(Ga) ratios. The band around 265 cm^{-1} is related to the metal bonds of [Ga(Ge)–Ga(Ge)] and occurred at x = 0.2 but not at x = 0.1, indicating the formation of a sulfur-deficient environment in the glass network. The increasing bands near 345 and 408 cm^{-1} were associated with the vibrations of edge- or corner-shared $[Ga(Ge)S_4]$ units. Interestingly, the band at 212 cm^{-1} was related to the covalent bonds of Ag–S and was observed at x = 0.1. This band then disappeared with decreasing amount of Sb component and Ga(Ge) units. The results indicated that a high

number of defect sites correlated with Ag^+ migration were possibly provided by the S-rich network[20-23].

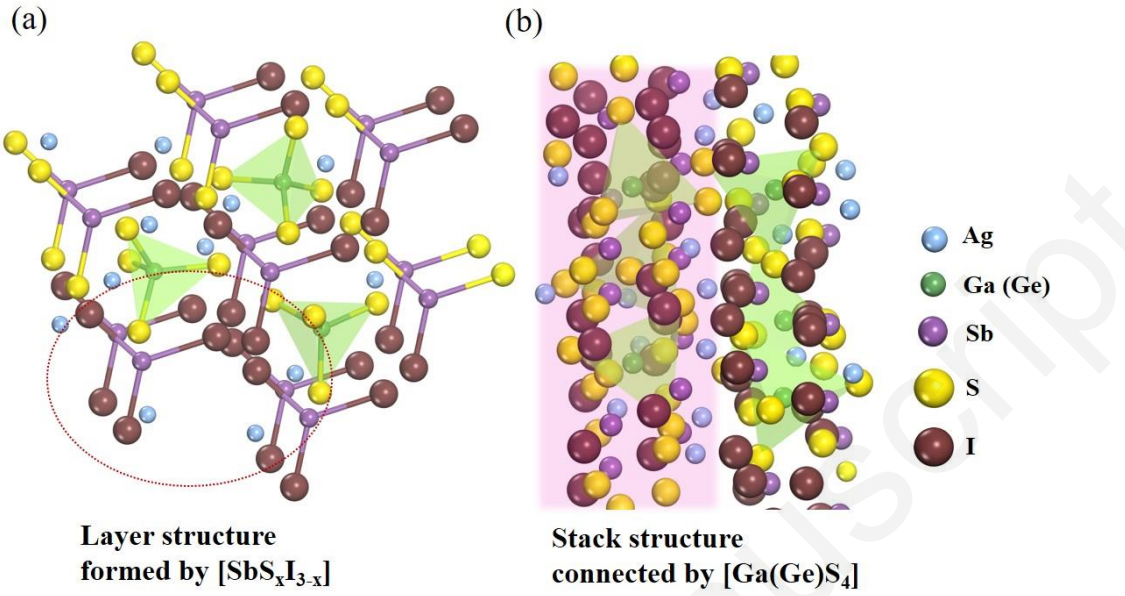

Fig. 6. Schematic diagram of the detailed ion transmission channel, top view of the "layer" structure in the ball stick model (a) and side view of the stack structure in the atomistic model (b).

Based on the evolution of network caused by the substitution, the specific formation of ionic channel and its effect on the ion's diffusion were reasonably evaluated. When a large amount of Sb was introduced into the network, I^- ions were more likely to combine with Sb ions, thereby forming the units of [SbS$_x$I$_{3-x}$], which enlarged the channel size and volume due to the large ionic radius. Meanwhile, the Ga(Ge) preferred to form the [Ga(Ge)S$_4$] tetrahedron in the S-rich environment, and their shared S^- bonds were expected to present two different behaviors in the network. First, the [SbS$_x$I$_{3-x}$] units were coordinated with bridging sulfur bonds given by [Ga(Ge)S$_4$] tetrahedron, which effectively prevented the aggregation of [SbSI] units, thereby preventing devitrification. However, abundant defect sites (i.e., unstable and active Ag–S bonds), which reduced the distance among the Ag^+ ions and decreased the activation energy, were provided by the non-bridging sulfur of [Ga(Ge)S$_4$] tetrahedron[24]. Accordingly, the [SbSI] units provided a ribbon stacking framework with chains connected by weak van der Waals forces. The chains in the same dimension were expected to intertwine into a net-like structure. Therefore, the entire ionic channel can be described

as the stacked structure formed by the loose and porous "net" layer-by-layer, as shown in Fig. 6. The pseudo tetrahedron of [SbS_xI_{3-x}] was assumed to be the planer structure, because its bond angle was close to 120°. Hence, in the short-range order, the interconnection of Sb-related units caused by bond energy and van der Waals can be regarded as the monolayers, as shown in Fig. 6 (a). The infinitely extended [SbS_xI_{3-x}] was linked by Ga(Ge) tetrahedron in three dimensions, as shown in Fig. 6 (b). Most of the Ag^+ ions were trapped in the defective sites created by NBS units of Ga(Ge) tetrahedron, whereas the rest occupied the interstitial sites and were randomly distributed around the I ions. These free carriers easily passed through the ionic channels because of their low activation energy. The Coulomb force attraction of anions was weakened by the defect sites, which were sufficiently close one another. The enlarged channel volume was caused by the loose multilayered structure. With continued incorporation of AgI in the optimized component, the concentration of conductive silver ions improved, further enhancing the conductive property of the glass electrolytes.

4. Conclusion

A-series samples of $60[x(Ga_2S_3–3GeS_2)–(1-4x)Sb_2S_3]–40AgI$ and B-series samples of $(100-y)(0.1Ga_2S_3–0.3GeS_2–0.6Sb_2S_3)–yAgI$ were prepared by vacuum melt method, and the solubility of AgI dopant was as high as 60 mol% in the optimized $(GG)Sb_{0.6}$ sample. The ion transport behavior and channel structures of Ag^+ conductors were studied. Notable superionic transport behavior and good thermal stability were shown by the B-series glasses. A relatively high room temperature conductivity of 2.955×10^{-3} S/cm was reported. The low activation energy (0.07 eV) of glassy samples confirmed the effectiveness of the migrating path in the optimized sample. Raman analysis suggested that the ion transmission channel was formed by the loose nets, which consisted of infinite connection of [$SbS_{3-x}I_x$] units, and the [$Ga(Ge)S_{4-x}I_x$] units conjoined single layers. Hence, the conductive ions of Ag^+ were easily activated to the concerted transport by occupying the defective and interstitial sites with a reduced migrating energy barrier. This work proposed a new quaternary structure of glassy electrolytes and provided insights into Ag^+

ions migration in the network for further research on solid-state batteries.

Acknowledgments

This work was financially supported by National Natural Science Foundation of China (Grant no. 51972176).

Reference

[1] R. Chen, Q. Li, X. Yu, L. Chen, H. Li, Approaching Practically Accessible Solid-State Batteries: Stability Issues Related to Solid Electrolytes and Interfaces, Chem Rev (2019). http://doi.org/10.1021/acs.chemrev.9b00268.

[2] Y. Kato, S. Hori, T. Saito, K. Suzuki, M. Hirayama, A. Mitsui, M. Yonemura, H. Iba, R. Kanno, High-power all-solid-state batteries using sulfide superionic conductors, Nature Energy 1(4) (2016) 16030. http://doi.org/10.1038/nenergy.2016.30.

[3] X. Yang, J. Luo, X. Sun, Towards high-performance solid-state Li-S batteries: from fundamental understanding to engineering design, Chem Soc Rev 49(7) (2020) 2140-2195. http://doi.org/10.1039/c9cs00635d.

[4] C. Zhou, S. Bag, V. Thangadurai, Engineering Materials for Progressive All-Solid-State Na Batteries, ACS Energy Letters 3(9) (2018) 2181-2198. http://doi.org/10.1021/acsenergylett.8b00948.

[5] Q. Zhang, D. Cao, Y. Ma, A. Natan, P. Aurora, H. Zhu, Sulfide-Based Solid-State Electrolytes: Synthesis, Stability, and Potential for All-Solid-State Batteries, Adv Mater 31(44) (2019) e1901131. http://doi.org/10.1002/adma.201901131.

[6] P.-J. Lian, B.-S. Zhao, L.-Q. Zhang, N. Xu, M.-T. Wu, X.-P. Gao, Inorganic sulfide solid electrolytes for all-solid-state lithium secondary batteries, Journal of Materials Chemistry A 7(36) (2019) 20540-20557. http://doi.org/10.1039/c9ta04555d.

[7] W. Fitzhugh, L. Ye, X. Li, The effects of mechanical constriction on the operation of sulfide based solid-state batteries, Journal of Materials Chemistry A 7(41) (2019) 23604-23627. http://doi.org/10.1039/c9ta05248h.

[8] J. Wan, J. Xie, D.G. Mackanic, W. Burke, Z. Bao, Y. Cui, Status, promises, and challenges of nanocomposite solid-state electrolytes for safe and high performance lithium batteries, Materials Today Nano 4 (2018) 1-16. http://doi.org/10.1016/j.mtnano.2018.12.003.

[9] Z. Zhu, I.-H. Chu, Z. Deng, S.P. Ong, Role of Na^+ Interstitials and Dopants in Enhancing the Na^+ Conductivity of the Cubic Na_3PS_4 Superionic Conductor, Chemistry of Materials 27(24) (2015) 8318-8325. http://doi.org/10.1021/acs.chemmater.5b03656.

[10] A. Sakuda, A. Hayashi, M. Tatsumisago, Metastable Materials for All-Solid-State Batteries, Electrochemistry 87(5) (2019) 247-250. http://doi.org/10.5796/electrochemistry.19-H0002.

[11] Q. Zhao, S. Stalin, C.-Z. Zhao, L.A. Archer, Designing solid-state electrolytes for safe, energy-dense batteries, Nature Reviews Materials 5(3) (2020) 229-252.

http://doi.org/10.1038/s41578-019-0165-5.

[12] C. Lin, E. Zhu, J. Wang, X. Zhao, F. Chen, S. Dai, Fast Ag-ion-conducting GeS_2–Sb_2S_3–AgI glassy electrolytes with exceptionally low activation energy, The Journal of Physical Chemistry C 122(3) (2018) 1486-1491. http://doi.org/10.1021/acs.jpcc.7b10630.

[13] B. Fan, H. Fu, H. Li, B. Xue, X. Zhang, Z. Luo, H. Ma, Ionic conductive GeS_2-Ga_2S_3-Li_2S-LiI glass powders prepared by mechanical synthesis, Journal of Alloys and Compounds 740 (2018) 61-67. http://doi.org/10.1016/j.jallcom.2017.12.356.

[14] A. Hayashi, N. Masuzawa, S. Yubuchi, F. Tsuji, C. Hotehama, A. Sakuda, M. Tatsumisago, A sodium-ion sulfide solid electrolyte with unprecedented conductivity at room temperature, Nat Commun 10(1) (2019) 5266. http://doi.org/10.1038/s41467-019-13178-2.

[15] M. Marple, D.C. Kaseman, S. Kim, S. Sen, Superionic conduction of silver in homogeneous chalcogenide glasses, Journal of Materials Chemistry A 4(3) (2016) 861-868. http://doi.org/10.1039/c5ta07301d.

[16] S. Stehlik, K. Shimakawa, T. Wagner, M. Frumar, Diffusion of Ag ions under random potential barriers in silver-containing chalcogenide glasses, Journal of Physics D: Applied Physics 45(20) (2012). http://doi.org/10.1088/0022-3727/45/20/205304.

[17] A. Ray Hilton. Chalcogenide Glasses for infrared optics. McGraw-Hill Companies, USA, (2010) 73-74.

[18] Z. Li, C. Lin, G. Qu, L. Calvez, S. Dai, X. Zhang, T. Xu, Q. Nie, Formation and properties of chalcogenide glasses based on GeS_2–Sb_2S_3–AgI system, Materials Letters 132 (2014) 203-205. http://doi.org/10.1016/j.matlet.2014.06.083.

[19] G. Tang, C. Liu, L. Luo, W. Chen, Thermal properties, microstructure, and conductivity of new glasses based on the $GeSe_2$-Ga_2Se_3-AgI system, Journal of the American Ceramic Society 91(12) (2008) 4171-4174. http://doi.org/10.1111/j.1551-2916.2008.02816.x.

[20] H.-T. Guo, M.-J. Zhang, Y.-T. Xu, X.-S. Xiao, Z.-Y. Yang, Structural evolution study of additions of Sb_2S_3 and CdS into GeS_2 chalcogenide glass by Raman spectroscopy, Chinese Physics B 26(10) (2017) 255-261. http://doi.org/10.1088/1674-1056/26/10/104208.

[21] M. Zhang, Z. Yang, L. Li, Y. Wang, J. Qiu, A. Yang, H. Tao, D. Tang, The effects of germanium addition on properties of Ga-Sb-S chalcogenide glasses, Journal of Non-Crystalline Solids 452 (2016) 114-118. http://doi.org/10.1016/j.jnoncrysol.2016.08.023.

[22] C. Lin, Z. Li, L. Ying, Y. Xu, P. Zhang, S. Dai, T. Xu, Q. Nie, Network Structure in GeS_2–Sb_2S_3 Chalcogenide Glasses: Raman Spectroscopy and Phase Transformation Study, The Journal of Physical Chemistry C 116(9) (2012) 5862-5867. http://doi.org/10.1021/jp208614j.

[23] M. Ichikawa, T. Wakasugi, K. Kadono, Glass formation, physico-chemical properties, and structure of glasses based on Ga_2S_3–GeS_2–Sb_2S_3 system, Journal of Non-Crystalline Solids 356(43)

(2010) 2235-2240. http://doi.org/10.1016/j.jnoncrysol.2010.08.029.

[24] D.S. Patil, M. Konale, S. Cozic, L. Calvez, V. Zima, T. Wagner, J.S. McCloy, D. Le Coq, Percolation behavior of Ag in $Ge_{16}Sb_{12}Se_{72}$ glassy matrix and its impact on corresponding ionic conductivity, Journal of Alloys and Compounds 782 (2019) 375-383. http://doi.org/10.1016/j.jallcom.2018.12.140.